*buildings*

MDPI

*Article*

# Multi-Objective Optimization of UHPC Infill Strengthening for Arch Bridges Based on Finite Element Response Mapping and NSGA-III

**Xiaoqing Liu [1], Jing Zhao [1], Yunchao Zheng [1] and Youliang Ding [2,*]**

[1] Huadong Engineering Corporation Limited, PowerChina, Hangzhou 311122, China; liu_xq4@hdec.com (X.L.); zhao_j10@hdec.com (J.Z.); zheng_yc@hdec.com (Y.Z.)
[2] Key Laboratory of Concrete and Prestressed Concrete Structures of Ministry of Education, Southeast University, Nanjing 210096, China
* Correspondence: civilding@seu.edu.cn

## Abstract

To address the difficulty of coordinating structural performance improvement, material consumption control, and construction feasibility in the strengthening design of existing small-span concrete arch bridges, this study proposes a multi-objective optimization method for determining the ultra-high performance concrete (UHPC) infill strengthening thickness based on finite element response mapping and non-dominated sorting genetic algorithm III (NSGA-III). An existing multi-rib concrete arch bridge is taken as the engineering case. Field inspection, load testing, finite element model calibration, and comparative analysis of typical strengthening configurations are first conducted to clarify the applicability of the overall UHPC infill strengthening scheme. The maximum control thickness of UHPC infill between arch ribs is then selected as the primary design variable. A three-objective performance–material-consumption optimization model is established by minimizing mid-span deflection, maximum compressive stress at the arch springing, and UHPC consumption. The non-dominated candidate solution set is obtained using the NSGA-III algorithm combined with finite element response mapping. Representative finite element results show that the mid-span deflection and arch-springing compressive stress of the unstrengthened structure are 12.59 mm and 10.33 MPa, respectively. When the UHPC infill thickness is controlled within the range of 230.90–251.00 mm, the mid-span deflection decreases to 7.38–7.77 mm, and the arch-springing compressive stress decreases to 6.64–7.36 MPa. The optimization results indicate that structural deformation and critical-section stress generally decrease with increasing UHPC consumption, whereas the mechanical benefit gradually diminishes in the high-consumption range. Among the six reported cases, the 241 mm case represents a compromise between calculated structural responses and UHPC consumption under the modeled loading condition. This scheme corresponds to a mid-span deflection of 7.52 mm, an arch-springing compressive stress of 6.82 MPa, and a UHPC consumption of 19.83 $m^3$, representing reductions of approximately 40.27% and 33.98% in deflection and stress, respectively, compared with the unstrengthened state. The findings provide a case-specific quantitative basis for the strengthening design of the investigated bridge and may serve as a reference for similar small-span multi-rib concrete arch bridges under comparable conditions.

**Keywords:** existing concrete arch bridge; UHPC infill strengthening; finite element response mapping; NSGA-III; multi-objective optimization; Pareto front

Check for updates

Academic Editor: Leandro Fleck Fadel Miguel

Received: 9 September 2026
Revised: 26 October 2026
Accepted: 3 November 2026
Published: 5 November 2026

**Copyright:** © 2026 by the authors. Licensee MDPI, Basel, Switzerland. This article is an open access article distributed under the terms and conditions of the Creative Commons Attribution (CC BY) license.

## 1. Introduction

Under the combined effects of long-term service, environmental erosion, increasing traffic loads, and insufficient maintenance, small- and medium-span concrete arch bridges are prone to material aging, stiffness degradation, local cracking, insufficient load-bearing reserve, and reduced durability [1,2]. For aged arch bridges that still serve traffic or landscape functions, demolition and reconstruction are often constrained by traffic organization, construction cost, environmental disturbance, and preservation of historical or contextual features. Therefore, rational strengthening and service-life extension are more consistent with engineering practice and the concept of green construction [3]. Although arch bridges are primarily characterized by axial compression, their actual structural response is affected by arch-springing thrust, mid-span deflection, transverse interaction, local damage, and interface deterioration [4]. Strengthening designs that rely only on empirical judgment or a single evaluation index may therefore lead to either insufficient safety reserve or excessive material consumption.

Traditional strengthening methods for arch bridges mainly include section enlargement, steel plate bonding, fiber-reinforced composite bonding, arch-wave closure, core filling, and the addition of transverse connections. Drosopoulos et al. analyzed FRP strengthening of stone arch bridges and showed that fiber-reinforced materials can improve flexural capacity and ductility of arch structures [5]. Sumon summarized the application scenarios of steel components, carbon-fiber plates, and tensioned cable systems in the strengthening of masonry arch bridges [6]. Zhang et al. verified the contribution of CFRP rebars to shear resistance and overall stability of stone arch bridges through field testing and finite element modeling [7]. For reinforced concrete arch bridges, Scattarreggia et al. emphasized through collapse analysis that strengthening design should account for damage evolution and structural limit states [8], while Yuan et al. demonstrated the necessity of differentiated strengthening of local components in aged arch bridges from the perspective of hanger reinforcement [9]. Domestic studies have also provided useful findings on internal force calculation for composite sections, strengthening methods for double-curved arch bridges, new connection configurations, and practical engineering applications [10,11]. Related engineering experience further indicates that arch bridge strengthening schemes should simultaneously consider local stress improvement and overall load-transfer coordination [12–14]. These studies provide an important foundation for arch bridge strengthening. International studies have also reported a field-investigation- and numerical-model-based assessment and strengthening design for an existing reinforced-concrete arch bridge in Sarajevo [15], experimental and analytical evaluation of externally bonded composite strengthening for reinforced-concrete arches [16], and a low-mass tuned mass damper strategy for seismic retrofitting of a reinforced-concrete arch bridge [17]. Together, these studies provide a broader basis for arch-bridge assessment and strengthening, while the present study focuses on optimizing ultra-high performance concrete (UHPC) infill thickness with respect to static structural response and material consumption. However, conventional materials and local strengthening methods may still involve increased self-weight, insufficient interface durability, high sensitivity to construction quality, local stiffness discontinuities, and relatively high long-term maintenance costs.

Ultra-high-performance concrete (UHPC) has high compressive strength, high toughness, low permeability, and excellent durability, and has attracted increasing attention in the repair and strengthening of existing bridges. Wang et al. applied UHPC to the strengthening of existing stone arch bridges and indicated that thin UHPC layers can enhance structural load-bearing capacity with a limited increase in thickness [18]. Yang et al. conducted full-scale tests on damaged RC arches and showed that UHPC strengthening can delay crack development and improve ultimate bearing capacity [19]. Song et al. reported that

composite interface treatments, including surface roughening, adhesive coating, and planting reinforcement, are beneficial for improving the cooperative behavior between UHPC and existing concrete [20]. Studies on UHPC material properties, design recommendations, and engineering applications also provide important references for strengthening existing structures [21,22]. Relevant technical reports and material characterization studies further confirm the advantages of UHPC in terms of strength, toughness, and durability [23,24]. In addition, experimental studies on UHPC–normal concrete composite members indicate that interface bonding and structural connection details play important roles in composite mechanical behavior [25,26]. Therefore, UHPC strengthening design should not only consider the material strength advantage, but should also emphasize the coordination among structural efficiency, interface reliability, and material consumption.

Parameter design for bridge strengthening is essentially a multi-objective decision-making problem. On the one hand, a strengthening scheme should reduce critical-section stress, control mid-span deflection, and improve overall structural stiffness. On the other hand, it should control UHPC consumption and construction complexity. Traditional single-objective optimization usually aggregates multiple indicators into a single comprehensive index through weighting, but the selection of weights is highly subjective and cannot adequately reveal the trade-off relationship between structural performance and material consumption. García-Segura et al. applied metamodel-assisted multi-objective optimization to sustainable bridge design, demonstrating the applicability of multi-objective decision-making in bridge engineering [27]. Non-dominated sorting genetic algorithm III (NSGA-III) improves the distribution of solution sets in three-objective and higher-dimensional objective spaces through a reference-point mechanism [28], while Non-dominated sorting genetic algorithm II (NSGA-II) provides the fundamental framework of non-dominated sorting and elitist preservation [29]. In addition, studies on normal-boundary intersection, comparisons of multi-objective evolutionary algorithms, and multi-objective optimization theory provide methodological foundations for the construction of Pareto solution sets [30–32]. Bridge management and life-cycle optimization studies also indicate that safety, economy, and durability should be considered within a unified decision-making framework [33,34].

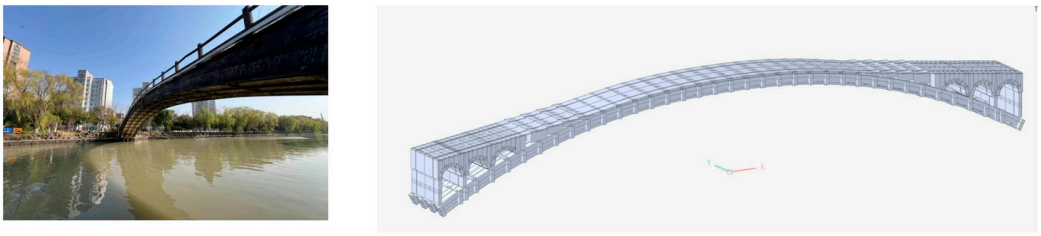
Based on the above considerations, this study focuses on the overall UHPC infill strengthening of an existing small-span multi-rib concrete arch bridge and investigates the influence of infill thickness on structural performance and material consumption. The main work of this study includes clarifying the strengthening demand of the existing arch bridge through field inspection and finite element calibration; determining the overall UHPC infill scheme through comparative analysis of typical strengthening configurations; constructing thickness–response mappings based on finite element parametric results; establishing a three-objective optimization model involving mid-span deflection, arch-springing compressive stress, and UHPC consumption; and obtaining the non-dominated solution set using NSGA-III. Finally, the recommended strengthening thickness is determined by considering safety reserve, material consumption, construction feasibility, and parameter robustness.

## 2. Engineering Case and Finite Element Analysis Basis

### *2.1. Engineering Overview and Existing Structural Condition*

The investigated structure is an existing small-span multi-rib concrete arch bridge, as shown in Figure 1. The bridge has a total length of 33.53 m and a deck width of 3.23 m, and it crosses a river channel. It has been in service for a long period, while its original design and construction documents are incomplete. Field inspection and load testing indicate that the structure exhibits evident stiffness degradation, local cracking, and insufficient load-bearing reserve. In the static load test, the calibration coefficient of some strain measurement points reached 1.01, and the mid-span deflection calibration coefficient reached 1.23. The

maximum relative residual strain was 34.69%, and the relative residual mid-span deflection was 21.45%. These results indicate that the original bridge requires strengthening in terms of both serviceability and critical-section mechanical performance. The interpretation of load test results and design control indicators follows the relevant specifications for highway bridge load testing and bridge design [35,36].



(a) Site bridge (b) 3D finite element model

**Figure 1.** Field view of the bridge and the three-dimensional finite element model.

The static load test was conducted using water-filled tanks placed on the bridge deck. The planned loading consisted of six increments of 1.5 kN/m$^2$, reaching a maximum of 9.0 kN/m$^2$. The reported measurements cover the first four loading levels, up to 6.0 kN/m$^2$, followed by unloading. Arch-springing strains were monitored using temperature-compensated strain gauges connected to a wireless acquisition system, while vertical deflection at the crown was measured using a precision level. Each loading level was maintained for 5–15 min, and residual responses were measured 10–15 min after unloading.

Dynamic testing was also conducted using ambient vibration measurements without traffic loading on the bridge. Vertically oriented magnetoelectric vibration sensors installed on the deck were connected to a dynamic signal acquisition system to record the response under ambient excitation. The measured frequency spectrum exhibited a peak at approximately 3.93 Hz.

From the perspective of structural behavior, the damage characteristics of this type of small-span multi-rib arch bridge are commonly reflected in nonuniform force transfer among arch ribs, stress concentration at the arch springing, excessive mid-span deflection, and insufficient transverse integrity. If strengthening is applied only to local regions, it may be difficult to effectively improve the overall load-transfer path. Conversely, if an overall wrapping or box-section strengthening scheme with high material consumption is adopted, construction complexity and material cost may increase significantly. Therefore, this study considers strengthening scheme selection and parameter optimization within a unified framework, with particular attention to a UHPC infill strengthening configuration that balances structural efficiency and engineering economy.

### *2.2. Overall UHPC Infill Strengthening Scheme and Optimization Object*

In the preliminary comparison of strengthening schemes for the same engineering object, conventional UHPC jacketing at the arch soffit, UHPC backfill above the arch, and closed arch-wave box strengthening all showed certain limitations in applicability. Although the arch-soffit jacketing scheme has a relatively direct construction procedure, it may easily cause local stiffness discontinuities and interface stress concentration along the lower edge of the arch ribs. The arch-back backfill scheme has a limited unloading effect on the critical stress region near the arch springing. The closed arch-wave box scheme can improve the overall stiffness, but it requires greater material consumption and more demanding formwork control, and it may increase the difficulty of subsequent inspection and maintenance. The engineering background, damage condition, design variable, and optimization method are summarized in Table 1.

**Table 1.** Overview of the engineering background and optimization object.

| Item | Description |
| --- | --- |
| Bridge type | Existing small-span multi-rib concrete arch bridge |
| Main structural deficiencies | Stiffness degradation, excessive mid-span deflection, stress concentration at the arch springing, and insufficient load-bearing reserve |
| Strengthening scheme | Overall UHPC infill strengthening between arch ribs |
| Design variable | Maximum control thickness of UHPC infill, h |
| Target responses | Mid-span deflection, maximum compressive stress at the arch springing, and UHPC material consumption |
| Optimization method | Finite element response mapping and NSGA-III multi-objective optimization |

Based on the above comparison, the overall UHPC infill strengthening scheme is selected as the optimization object in this study. In this scheme, UHPC is filled into the arch-shaped cavities between arch ribs and other critical load-transfer regions, transforming the originally discrete load-transfer path of local arch ribs into a more continuous cooperative force-transmission system. This helps reduce stress concentration at the arch springing and enhance the overall structural stiffness. Because the UHPC infill control thickness directly affects the contribution of the strengthening layer to structural resistance, material consumption, and on-site construction feasibility, it is selected as the key design parameter. The specific optimization procedure is shown in Figure 2.

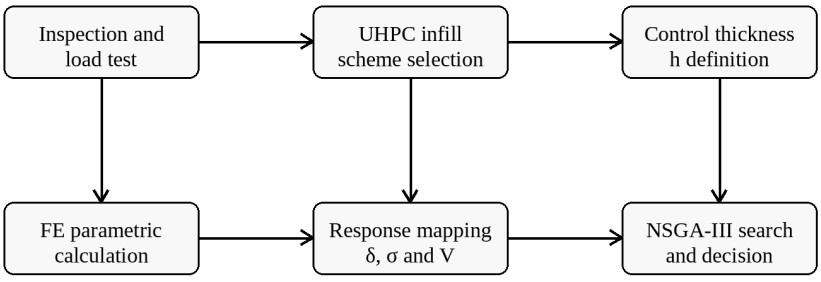



**Figure 2.** Framework for multi-objective optimization of UHPC infill strengthening thickness.

It should be noted that the UHPC infill thickness discussed in this study does not refer to a uniform strengthening layer thickness applied throughout the entire bridge, but to the maximum control thickness within the arch-shaped cavity between arch ribs. In actual construction, the UHPC infill boundary should vary naturally with the existing cavity geometry, arch-rib profile, and local load-transfer demand. Therefore, UHPC consumption is not simply equivalent to a linear function of thickness, but it should be jointly determined by the maximum control thickness and the actual geometric boundary of the infill region. This clarification is important for interpreting the relationship among thickness, volume, and structural response in the subsequent analysis.

### *2.3. Finite Element Model Establishment and Calibration*

Six strengthened three-dimensional solid models were identified in the archived Abaqus database. Each model comprises the existing bridge body and one UHPC infill body. The existing concrete was represented using the concrete damaged plasticity

(CDP) model, whereas the UHPC was represented as an isotropic linear-elastic material. Reinforcing steel was not discretized as separate elements in the six active model assemblies. The existing bridge body used ten-node quadratic tetrahedral solid elements (C3D10). The p0 infill used six-node wedge elements (C3D6) and eight-node reduced-integration brick elements (C3D8R), while the p1–p5 infills used C3D8R elements. Tables 2 and 3 report the material inputs and case-specific discretization.

**Table 2.** Material properties and CDP inputs used in the archived finite-element models.

| Material | Constitutive Model | Density | Elastic Modulus | Poisso |
|---|---|---|---|---|
| Existing concrete | CDP | $2.4 \times 10^{-9}$ | 32,599.8 | 0.20 |
| UHPC infill | Isotropic linear elastic | $2.6 \times 10^{-9}$ | 42,450 | 0.19 |

Note: The CDP parameters for the existing concrete were: dilation angle $\psi = 30°$, eccentricity $\in = 0.1$, $\sigma_{b0}/\sigma_{c0} = 1.16$, $K_c = 0.667$, and viscosity parameter $\mu = 0.005$.

**Table 3.** Comparison of the six strengthened solid models.

| Model | UHPC Volume ($m^3$) | UHPC Element Type | Mesh Seed (mm) | Total Elements | Gravity Region |
|---|---|---|---|---|---|
| p0 | 17.67 | C3D6 + C3D8R | 200 | 31,247 | Both |
| p1 | 18.22 | C3D8R | 200 | 32,015 | Existing bridge |
| p2 | 18.76 | C3D8R | 200 | 33,935 | Both |
| p3 | 19.76 | C3D8R | 200 | 32,207 | Both |
| p4 | 20.94 | C3D8R | 200 | 32,399 | Both |
| p5 | 22.29 | C3D8R | 150 | 37,135 | Both |

Note: All six models share the same existing bridge geometry and C3D10 mesh, material definitions, support conditions, Tie interface, and geometrically nonlinear static analysis. "Both" denotes the existing bridge and UHPC infill.

All six models were analyzed using a single geometrically nonlinear static step in Abaqus. Gravity was applied in the negative global Y-direction with an acceleration input of 10,000, and a uniform pressure with an input value of 0.04 was applied to the upper loading surface. At both ends, the support surfaces were kinematically coupled to reference points that were fully fixed. The old concrete–UHPC interface was represented by a Tie constraint, corresponding to an idealized fully bonded interface without relative slip. The analysis represents the completed strengthened state.

To contextualize the pressure magnitude, a supplementary retrospective comparison was performed using an estimated equivalent self-weight pressure $G_{eq} = 26.24$ kN/m$^2$ and the recorded fourth-stage test load $Q_{test} = 6$ kN/m$^2$. Applying factors of 1.2 and 1.4, respectively, gives:

$$\begin{aligned} q_{cmp} &= 1.2G_{eq} + 1.4Q_{test} \\ &= (1.2 \times 26.24 + 1.4 \times 6)\text{kN/m}^2 \\ &= 39.888\text{kN/m}^2 \\ &= 0.039888\ \text{MPa} \approx 0.04\ \text{MPa}. \end{aligned} \quad (1)$$

A separate Midas Civil beam-element model was used for the self-weight comparison with the Abaqus solid model. The beam model represents bridge members using one-dimensional line elements with assigned material and cross-sectional properties. In contrast, the six strengthened Abaqus models (p0–p5) discretize the existing bridge and UHPC infill volumes using three-dimensional solid elements to obtain continuum displacement and stress fields. Under the self-weight condition, the maximum crown displacements obtained from the Midas model and the Abaqus solid model were 2.262 mm and 2.327 mm, respectively, while the corresponding maximum compressive stresses were 2.267 MPa and

2.329 MPa. The relative errors were 2.87% and 2.73%, respectively. These errors are within an acceptable range for engineering analysis, indicating that the finite element model can serve as a reliable data basis for subsequent thickness parametric analysis and multi-objective optimization.

The calibration described above verifies numerical consistency between the solid and beam models under self-weight; however, further validation against field measurements is necessary. The load test reported in Section 2.1 recorded a mid-span deflection calibration coefficient of 1.23 and a maximum strain calibration coefficient of 1.01, indicating that measured responses exceeded the reference theoretical values by 23% and 1%, respectively. The Abaqus model predicts a mid-span deflection of 12.59 mm for the unstrengthened structure under equivalent service load. Applying the calibration coefficient of 1.23 yields an implied measured deflection of approximately 15.5 mm, which is consistent with the stiffness-degradation trend suggested by the high calibration coefficient. Similarly, the predicted arch-springing compressive stress of 10.33 MPa aligns with the strain calibration coefficient of 1.01. These comparisons indicate that the model captures the correct response magnitude relative to field observations, supporting its use for parametric analysis.

### *2.4. Representative Thickness Cases and Original Response Data*

To investigate the effects of UHPC infill thickness on structural response and material consumption, the thickness optimization range was set first. By taking into account construction feasibility, the geometry of the existing cavity, and structural load-transfer requirements, the thickness optimization range of 230–260 mm was determined. The lower limit was selected to guarantee constructability and sufficient load transfer, whereas the upper limit was constrained by the cavity dimensions and practical implementation considerations. The mid-span deflection, arch-springing compressive stress, and UHPC volume consumption under different representative cases were then obtained using the Abaqus finite element model. The original calculation results include six representative strengthening cases and one unstrengthened reference case. In this study, all data were organized strictly according to the original finite element outputs and geometric statistics, as listed in Table 4. The maximum arch-springing compressive stress was extracted from the minimum-principal-stress field (S, Min. Principal) within the arch-springing region adjacent to the fixed support. At the end of the static analysis step, element integration-point stresses were extrapolated and averaged at the nodes using a 75% averaging threshold, and the absolute magnitude of the most negative value was reported. The same procedure was applied to all cases.

The scheme numbers in Table 4 are used only to distinguish representative finite element cases and do not indicate a strictly equally spaced thickness sequence. The mid-span deflection, arch-springing compressive stress, and UHPC consumption of each scheme were obtained from the finite element model and the actual infill geometry statistics. Because the infill boundary is affected by the existing cavity shape and local structural constraints, the material consumption is jointly determined by the maximum control thickness and the geometric extent of the infill region. Therefore, it is not simplified as a linear function of thickness. This treatment helps ensure the engineering traceability of the optimization data and avoids oversimplifying the irregular strengthening configuration into an idealized uniform-section problem.

**Table 4.** Representative calculation results for different UHPC infill strengthening thicknesses.

| Scheme | Mid-Span Deflection/mm | Arch-Springing Compressive Stress/MPa | UHPC Consumption/$m^3$ | Strengthening Thickness/mm |
|---|---|---|---|---|
| Unstrengthened | 12.59 | 10.33 | 0 | 0 |
| Scheme 1 | 7.77 | 7.36 | 17.71 | 230.90 |
| Scheme 2 | 7.73 | 6.96 | 18.23 | 234.00 |
| Scheme 3 | 7.69 | 6.85 | 18.81 | 236.50 |
| Scheme 4 | 7.52 | 6.82 | 19.83 | 241.00 |
| Scheme 5 | 7.48 | 6.77 | 20.89 | 246.00 |
| Scheme 6 | 7.38 | 6.64 | 22.31 | 251.00 |

Note: The data in the table are organized based on the original finite element calculations and geometric statistical results. The scheme numbers are used only to distinguish representative cases and do not indicate a strictly equally spaced thickness sequence.

## 3. Performance–Material-Consumption Multi-Objective Optimization Method

### *3.1. Design Variables, Objective Functions, and Constraints*

The maximum control thickness of UHPC infill is a key parameter affecting structural performance and material consumption. If the thickness is too small, the UHPC layer may not sufficiently participate in the overall load-bearing mechanism, resulting in limited reductions in arch-springing stress and mid-span deflection. Conversely, excessive thickness may lead to material redundancy, increased construction difficulty, and reduced economic efficiency. In this study, the maximum control thickness h of UHPC infill between arch ribs is selected as the primary design variable, with a value range of 230–260 mm. This interval covers the main thickness range considered in the finite element parametric analysis and also satisfies the basic feasibility requirements for formwork erection, casting, and interface treatment in small-span arch bridge strengthening.

The multi-objective optimization model consists of three objective functions. First, the maximum mid-span deflection $\delta(\mathrm{h})$ is minimized to characterize the overall structural stiffness and serviceability. Second, the maximum compressive stress at the arch springing $\sigma(\mathrm{h})$ is minimized to characterize the safety reserve and stress concentration level in the critical compression region. Third, the UHPC volume $\mathrm{V}(\mathrm{h})$ is minimized to characterize material consumption. For the representative schemes considered, deflection and arch-springing compressive stress vary in the same direction. The principal conflict is therefore between reductions in these mechanical responses and the increase in UHPC consumption. Therefore, no single scheme can simultaneously minimize all three objectives.

$$\min_h \mathbf{F}(h) = [f_1(h), f_2(h), f_3(h)]^{\mathrm{T}} = [\delta(h), \sigma(h), V(h)]^{\mathrm{T}} \tag{2}$$

$$\begin{cases} 230\mathrm{mm} \le h \le 260\mathrm{mm} \\ \delta(h) \le \delta_{\lim} \\ \sigma(h) \le \sigma_{\lim} \end{cases} \tag{3}$$

where $\delta(h)$ denotes the maximum mid-span deflection after strengthening, $\sigma(h)$ denotes the maximum compressive stress at the arch-springing section, and $V(h)$ denotes the UHPC material volume. $\delta_{\lim}$ and $\sigma_{\lim}$ are the control limits for deformation and stress restricted by bridge design codes, with numerical values of 36 mm and 13.8 MPa, respectively. Equation (2) represents the three-objective minimization problem, while Equation (3) defines the basic constraints for serviceability and strength safety.

### *3.2. Response Mapping Framework*

To avoid directly equating a limited number of discrete finite element cases with continuous optimization results, this study adopts a data chain consisting of finite element parametric calculation, response mapping, and multi-objective search. Specifically, field inspection is used to identify the necessity of strengthening; finite element scheme comparison is used to determine the overall UHPC infill configuration; parametric finite element calculations are performed to obtain mechanical responses and material consumption under different infill control thicknesses; and a mapping relationship between thickness and objective functions is then constructed based on these response data to provide objective-function evaluations for the NSGA-III search.

In the response mapping process, the mid-span deflection $\delta(h)$, arch-springing compressive stress $\sigma(h)$, and UHPC consumption $V(h)$ are taken as three output responses. For $\delta(h)$ and $\sigma(h)$, the mapping relationship should preserve the engineering trend that structural responses generally decrease as the strengthening contribution increases. For $V(h)$, because the infill region is affected by irregular cavity boundaries and local structural details, the material-consumption objective should be established according to actual geometric statistics rather than being forcibly assumed as a strictly linear function of $h$. The representative cases listed in Table 4 are used to compare the reported responses, support engineering interpretation, and select typical decision-making schemes. The response mapping adopted in this study mainly serves as a data interface between representative finite element cases and the optimization search. Its role is to reflect the overall trends of structural response and material consumption with thickness variation, rather than to replace refined finite element parametric analysis.

$$[\delta(h), \sigma(h), V(h)] = \mathbf{R}(h; \mathcal{D}_{\mathrm{FE}}) \tag{4}$$

where $\mathbf{y}(h)$ is the target response vector corresponding to the candidate thickness $h$, $\mathcal{D}_{\mathrm{FE}}$ is the finite element parametric dataset, and $\mathbf{R}$ is the response mapping function constructed from the finite element results. This mapping provides objective-function values for individuals in NSGA-III. Equation (3) schematically represents this relationship rather than specifying an explicit interpolation or regression equation.

This treatment distinguishes the functions of the two types of data. The representative finite element cases provide a numerical basis for structural response analysis, while the non-dominated solution set obtained by NSGA-III is used to reveal the trade-off relationship between performance indicators and material consumption.

### *3.3. NSGA-III Procedure and Rationale*

NSGA-III is a non-dominated sorting genetic algorithm based on a reference-point mechanism and is suitable for three-objective and higher-dimensional optimization problems. Unlike traditional single-objective weighted optimization, NSGA-III does not require subjective weights to be specified in advance. Instead, it identifies the Pareto-optimal solution set through non-dominated relationships and maintains the distribution uniformity of the solution set in the objective space using the reference-point mechanism. Its basic procedure includes population initialization, objective-function evaluation, fast non-dominated sorting, reference-point-based normalization and association, niche selection, crossover and mutation, and elitist preservation. The main parameter settings of NSGA-III are listed in Table 5.

**Table 5.** Main parameter settings of the NSGA-III algorithm.

| Parameter | Value | Description |
|---|---|---|
| Population size | 50 | Ensures a basic distribution of the solution set |
| Maximum number of generations | 100 | Balances search sufficiency and computational efficiency |
| Crossover probability | 0.8 | Enhances the combinational search capability of candidate schemes |
| Mutation probability | 0.1 | Maintains population diversity and reduces the risk of local convergence |
| Number of objectives | 3 | Mid-span deflection, arch-springing stress, and UHPC consumption |

In the UHPC infill strengthening thickness optimization, each individual represents a candidate infill control thickness $h$, and its fitness is jointly determined by the mid-span deflection, the maximum compressive stress at the arch springing, and the UHPC consumption obtained from the response mapping model. First, non-dominated sorting is performed on the population, and solutions that are not dominated by any other individuals are assigned to the first non-dominated front. Then, the objective space is normalized and associated with uniformly distributed reference points, so that solutions with different objective preferences can be retained. Finally, an elitist preservation strategy is used to merge the parent and offspring populations, preferentially retaining individuals with better front ranks and more uniform distributions.

In non-dominated sorting, if one candidate scheme is no worse than another scheme in all objectives and is better in at least one objective, the former is considered to dominate the latter. NSGA-III screens individuals jointly through non-dominated ranking and reference-point association, enabling the solution set to cover candidate schemes with different engineering preferences, including economy-oriented, balanced, and performance-oriented schemes.

The algorithm parameters are set as follows: the population size is 50, the maximum number of iterations is 100, the crossover probability is 0.8, and the mutation probability is 0.1. For engineering optimization problems, the output of NSGA-III is not a single mathematical optimum, but a Pareto front and a set of candidate schemes with engineering interpretability. The final recommended scheme should be determined by further considering structural safety reserve, material consumption, construction feasibility, long-term durability, and parameter robustness.

### *3.4. Improvement Ratios and Engineering Decision Indicators*

To provide an intuitive comparison of the improvement in structural response before and after strengthening, the reduction ratios of mid-span deflection and arch-springing compressive stress are further defined in this study. These indicators are not involved in the NSGA-III search process but are mainly used for result interpretation and the engineering scheme comparison.

$$\eta_\delta = \frac{\delta_0 - \delta_h}{\delta_0} \times 100\%, \qquad \eta_\sigma = \frac{\sigma_0 - \sigma_h}{\sigma_0} \times 100\% \tag{5}$$

where $\eta_\delta$ and $\eta_\sigma$ denote the reduction ratios of mid-span deflection and arch-springing compressive stress, respectively; $\delta_0$ and $\sigma_0$ are the mid-span deflection and arch-springing compressive stress in the unstrengthened state, respectively; and $\delta_h$ and $\sigma_h$ are the mid-span

deflection and arch-springing compressive stress of the strengthened scheme corresponding to thickness $h$, respectively.

## 4. Results and Analysis

### *4.1. Influence of Thickness Parameters on Structural Response and Material Consumption*

According to the representative calculation results in Table 4, the mid-span deflection of all UHPC infill strengthening schemes is significantly lower than that of the unstrengthened state. The mid-span deflection of the unstrengthened structure is 12.59 mm, whereas that of the representative strengthened schemes decreases to 7.38–7.77 mm. This indicates that overall UHPC infill can effectively enhance the cooperative load-bearing capacity of arch ribs and improve the overall structural stiffness. In terms of arch-springing compressive stress, the value decreases from 10.33 MPa in the unstrengthened state to 6.64–7.36 MPa after strengthening, indicating that the infill strengthening scheme provides a stable unloading effect in the critical compression region.

Figure 3 shows the variations in mid-span deflection, arch-springing compressive stress, and UHPC consumption for the representative schemes. When the schemes are compared in ascending order of material consumption, they generally show a trend of increasing UHPC consumption accompanied by decreasing deflection and stress. However, the improvement in mechanical performance gradually diminishes. From Scheme 1 to Scheme 4, the UHPC consumption increases from 17.71 $m^3$ to 19.83 $m^3$, while the mid-span deflection decreases from 7.77 mm to 7.52 mm and the arch-springing compressive stress decreases from 7.36 MPa to 6.82 MPa, indicating a relatively evident improvement in mechanical performance. From Scheme 4 to Scheme 6, the UHPC consumption increases from 19.83 $m^3$ to 22.31 $m^3$, corresponding to an increase of approximately 12.51%. However, the deflection is further reduced by only about 1.86%, and the arch-springing compressive stress is further reduced by only about 2.64%. The calculated improvement ratios are listed in Table 6 and illustrated in Figure 4.

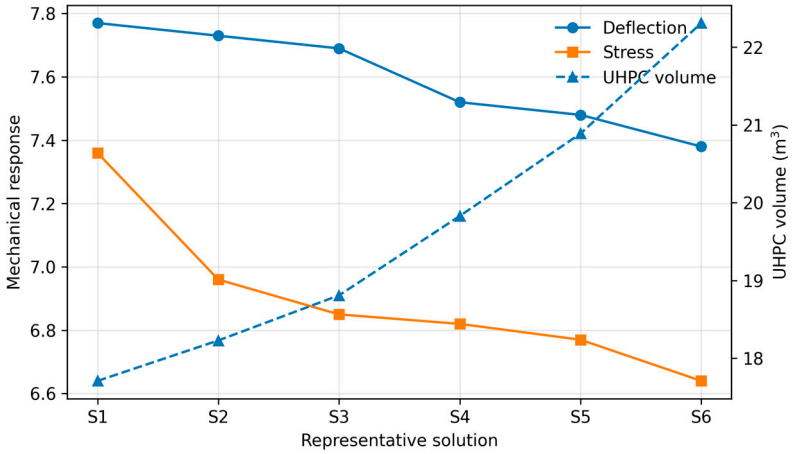



**Figure 3.** Variations in mid-span deflection, arch-springing compressive stress, and UHPC consumption under representative schemes.

These results reveal a diminishing marginal benefit in structural strengthening. When UHPC consumption is relatively low, the added material can effectively compensate for the insufficient sectional stiffness of the original structure and improve the local load-transfer path. Once a relatively stable cooperative load-bearing system has been formed in the infill region, further material addition mainly leads to redundancy, while its contribution to reducing stress and deflection becomes limited. Therefore, UHPC strengthening design

should not simply pursue increased thickness; instead, a balanced range with higher material utilization efficiency should be identified while satisfying the required safety reserve.

**Table 6.** Improvement ratios of representative strengthening schemes relative to the unstrengthened state.

| Scheme | Deflection Reduction Ratio/% | Arch-Springing Stress Reduction Ratio/% | UHPC Consumption/$m^3$ | Description |
|---|---|---|---|---|
| Scheme 1 | 38.28 | 28.75 | 17.71 | Low-consumption scheme |
| Scheme 2 | 38.60 | 32.62 | 18.23 | Representative solution |
| Scheme 3 | 38.92 | 33.69 | 18.81 | Representative solution |
| Scheme 4 | 40.27 | 33.98 | 19.83 | Recommended balanced scheme |
| Scheme 5 | 40.59 | 34.46 | 20.89 | Performance-oriented scheme |
| Scheme 6 | 41.38 | 35.72 | 22.31 | High-consumption performance-oriented scheme |

Note: The deflection reduction ratio and stress reduction ratio are calculated according to Equation (5).

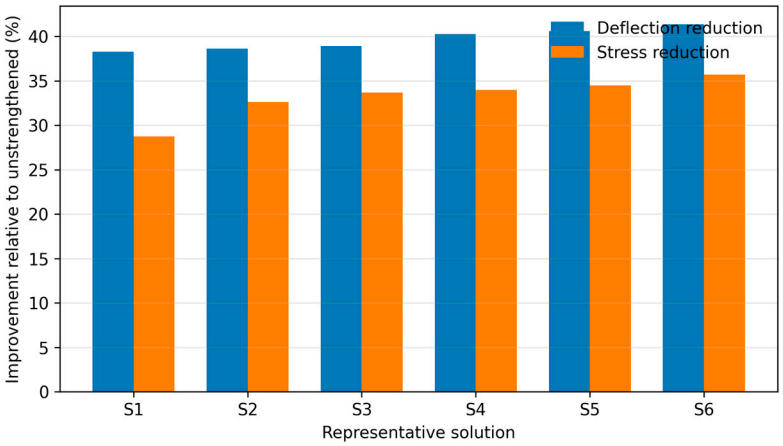



**Figure 4.** Mechanical performance improvement ratios of representative schemes relative to the unstrengthened state.

### *4.2. Trade-Off Relationship Among Deflection, Stress, and Material Consumption*

In the three-objective optimization, both mid-span deflection and arch-springing compressive stress are structural mechanical performance indicators, and they show an overall consistent improvement trend under the investigated conditions. Figure 5 presents the relationship between mid-span deflection and arch-springing compressive stress, where the marker size represents UHPC consumption. Figure 6 compares the normalized objective values of the representative schemes. For Figure 6, deflection, arch-springing stress, and UHPC volume were normalized separately using min–max normalization. It can be observed that schemes with smaller deflection generally correspond to lower arch-springing compressive stress, but they also require greater UHPC consumption. This indicates a trade-off between structural performance improvement and economic efficiency: schemes

with lower deflection and lower stress require more material, whereas schemes with lower material consumption usually retain higher deformation and stress levels.

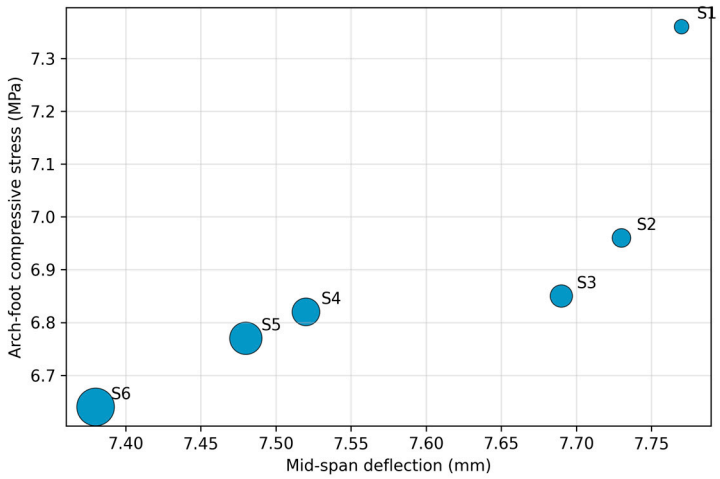



**Figure 5.** Trade-off relationship between mid-span deflection and arch-springing compressive stress.

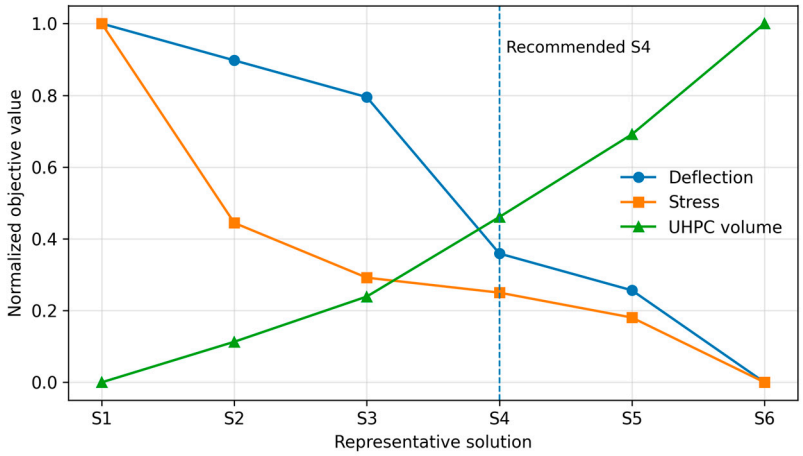



**Figure 6.** Comparison of normalized objective values of representative schemes.

From the perspective of engineering decision-making, Scheme 1 represents a low-material-consumption case, with a UHPC consumption of 17.71 $m^3$, a mid-span deflection of 7.77 mm, and an arch-springing compressive stress of 7.36 MPa. Although this scheme provides a significant improvement compared with the unstrengthened state, its arch-springing compressive stress remains relatively high among all strengthening schemes. Scheme 6 represents a performance-oriented scheme, with the deflection and stress reduced to 7.38 mm and 6.64 MPa, respectively, but its UHPC consumption reaches 22.31 $m^3$. If only structural response is considered, Scheme 6 is more favorable; however, when material utilization efficiency is taken into account, its performance–material-consumption coordination is not optimal.

Scheme 4 corresponds to a thickness of 241 mm, a UHPC consumption of 19.83 $m^3$, a mid-span deflection of 7.52 mm, and an arch-springing compressive stress of 6.82 MPa. Compared with Scheme 1, Scheme 4 reduces deflection by approximately 3.22% and stress by approximately 7.34%, while increasing material consumption by about 11.97%. Compared with Scheme 6, Scheme 4 sacrifices only about 1.86% in deflection improvement and 2.64% in stress improvement, but it reduces UHPC consumption by approximately 11.12%. These results indicate that Scheme 4 lies in a balanced region between performance improvement and material investment.

### *4.3. Pareto Front Partitioning and Determination of the Recommended Scheme*

The NSGA-III optimization produced 48 non-dominated solutions. Among these, the seven thickness values listed in Table 4 correspond to direct finite element calculations; the remaining 41 solutions are generated by the response mapping function described in Section 3.2, which interpolates between those seven data points. This distinction is indicated in Table 4 and preserved throughout the results: all deflection and stress values for the seven listed schemes are explicit Abaqus outputs, while intermediate thicknesses on the Pareto front are mapping-based interpolations that follow the same monotonic response trend.

In this study, the Pareto front is used to characterize the non-dominated relationships among different UHPC infill thickness schemes in terms of mid-span deflection, arch-springing compressive stress, and material consumption. Figure 7 is presented as a two-dimensional projection of the three-objective solution set onto the deflection–UHPC-consumption plane for visualizing the regional partitioning. The complete relationship among deflection, arch-springing compressive stress, and UHPC consumption is presented in Figure 5, where marker size represents UHPC consumption. Figure 8 compares the material increment and mechanical benefits when moving from Scheme 4 to Scheme 6. Since performance improvement is generally accompanied by increased UHPC consumption, a single scheme can hardly achieve the minimum deflection, minimum stress, and minimum material consumption simultaneously. Therefore, the significance of the Pareto solution set lies not in providing a unique optimal thickness, but in offering comparable candidate schemes for different engineering preferences.

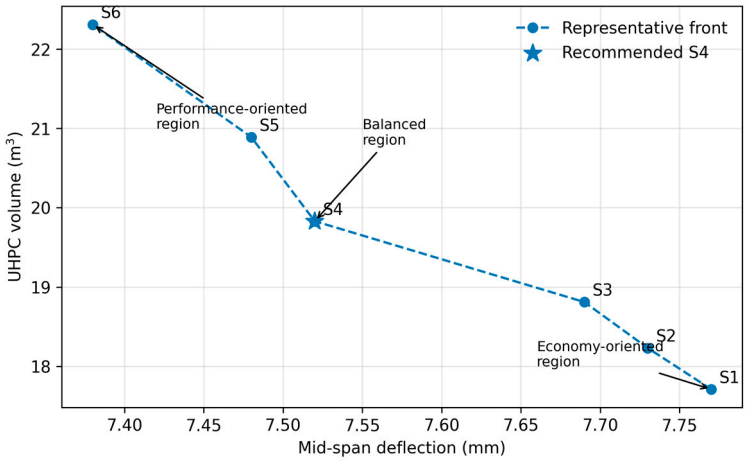



**Figure 7.** Partitioning of representative non-dominated schemes and the balanced optimal region.

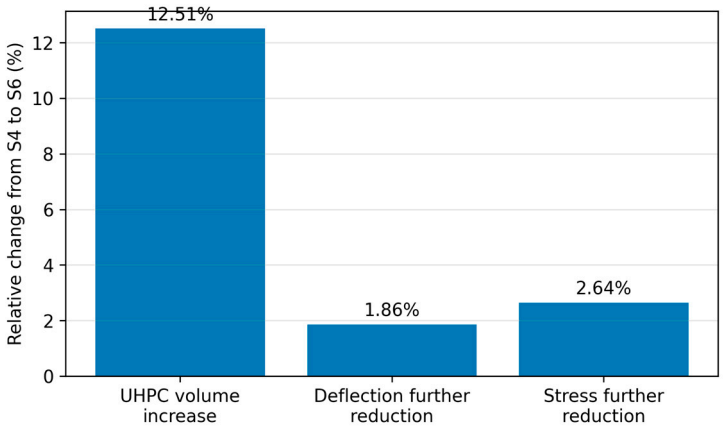



**Figure 8.** Comparison of marginal benefits when moving from Scheme 4 to Scheme 6.

Based on the non-dominated solution set and the characteristics of the representative schemes, the candidate schemes can be divided into an economy-oriented region, a balanced optimal region, and a performance-oriented region. The economy-oriented region is characterized by lower material consumption and is suitable for projects with strict budget constraints or relatively minor structural deficiencies, but its safety reserve is comparatively limited. The performance-oriented region provides better control of deflection and stress and is suitable for structures with higher risk levels or stricter deformation control requirements, but it involves higher material consumption and construction cost. The balanced optimal region achieves a better compromise between structural performance and engineering economy.

Considering the Pareto front distribution, representative scheme comparison, and construction feasibility, a UHPC infill thickness of 241 mm is recommended as the comprehensive optimal thickness in this study. This selection is supported by the diminishing-return pattern in Table 6: progressing from Scheme 1 (230.90 mm) to Scheme 4 (241 mm) reduces deflection by 3.22% and stress by 7.34%, while the subsequent step to Scheme 6 (251 mm) yields only 1.86% and 2.64% further improvement at the cost of 12.51% more material. Safety reserve is quantified by 40.27% deflection reduction and 33.98% stress reduction relative to the unstrengthened state. Construction feasibility is indicated by the position of 241 mm within the 230–260 mm range defined in Section 3.1. Robustness is reflected by response variations of at most 0.25 mm in deflection and 0.59 MPa in stress across adjacent schemes in the 236–246 mm subrange, confirming low sensitivity to minor deviations.

This thickness refers to the maximum control thickness within the arch-shaped cavity between arch ribs, rather than a uniform infill thickness applied throughout the entire bridge. In actual construction, the UHPC infill layer should be naturally formed along the arch-rib profile and cavity geometry, with the filling height gradually varying from the central region toward both sides to adapt to the existing bridge configuration and load-transfer path. This parameter has practical engineering significance, and its rationality should be jointly verified with the infill boundary, interface treatment, and construction process.

### *4.4. Engineering Applicability Analysis of the Recommended Scheme*

The representative schemes under different decision preferences are compared in Table 7. The engineering advantages of the recommended thickness of 241 mm are mainly reflected in four aspects. First, it provides a sufficient structural safety reserve. This scheme reduces the mid-span deflection from 12.59 mm in the unstrengthened state to 7.52 mm, corresponding to a reduction of approximately 40.27%, and decreases the arch-springing compressive stress from 10.33 MPa to 6.82 MPa, corresponding to a reduction of approximately 33.98%. Second, its material consumption remains at a moderate level. Compared with the performance-oriented Scheme 6, this scheme reduces UHPC consumption by approximately 2.48 $m^3$, corresponding to a reduction of about 11.12%, while only slightly sacrificing mechanical performance. Third, it has good construction feasibility. A thickness of 241 mm falls within an acceptable range for conventional casting and formwork control, facilitating on-site formwork erection, casting, self-compacting placement, and subsequent curing. Fourth, it exhibits favorable parameter robustness. The recommended scheme is located in a relatively stable region of objective variation and is not sensitive to small dimensional deviations during construction, making abrupt changes in structural response unlikely.

**Table 7.** Comparison of representative schemes under different decision preferences.

| Scheme Type | Representative Scheme | Main Indicators | Engineering Evaluation |
| --- | --- | --- | --- |
| Economy-oriented | Scheme 1 | h = 230.90 mm; δ = 7.77 mm; $\sigma$ = 7.36 Mpa; V = 17.71 $m^3$ | Low material consumption, but relatively high stress level; can be used as a low-cost reference scheme |
| Balanced optimal | Scheme 4 | h = 241.00 mm; δ = 7.52 mm; $\sigma$ = 6.82 Mpa; V = 19.83 $m^3$ | Balances mechanical performance, material consumption, and construction feasibility; recommended for application |
| Performance-oriented | Scheme 6 | h = 251.00 mm; δ = 7.38 mm; $\sigma$ = 6.64 Mpa; V = 22.31 $m^3$ | Provides the best mechanical response, but involves higher material consumption and construction cost, with limited marginal benefit |

From the perspective of long-term service, UHPC infill strengthening should not only satisfy short-term static performance requirements, but also account for shrinkage and creep, temperature effects, interface bond degradation, and environmental erosion. The recommended scheme avoids material redundancy and increased restraint effects caused by excessive thickening, while also preventing insufficient safety reserve associated with low-consumption schemes. Therefore, it is more consistent with the engineering principle of demand-oriented strengthening for aged arch bridges. If the design proceeds to the construction drawing stage, the local configuration can be further refined based on the measured cavity geometry, interface treatment method, and construction process.

## 5. Discussion

This study combines finite element parametric results with NSGA-III multi-objective optimization. Its core value lies in transforming the traditional strengthening design process from empirical thickness selection followed by checking for compliance the identification of performance–material-consumption trade-off relationships in a multi-objective space. For high-performance and high-cost materials such as UHPC, simply pursuing the optimal structural response is not necessarily reasonable from an engineering perspective. Only by simultaneously quantifying mid-span deflection, critical-section stress, and material consumption can the actual structural benefit per unit material input be evaluated, thereby reducing overly conservative design and material redundancy. Therefore, the present framework should be interpreted as a performance–material-consumption optimization rather than a direct cost optimization.

Compared with conventional single-objective optimization, NSGA-III does not output a unique optimal thickness, but rather a set of non-dominated schemes covering different engineering preferences. This form of result is more consistent with the practical decision-making requirements of existing bridge strengthening. For bridges with relatively minor deficiencies and strong budget constraints, economy-oriented schemes may be preferred. For bridges with higher risk levels or stricter deformation control requirements, performance-oriented schemes may be selected. For general strengthening projects, a balanced optimal scheme is more favorable for coordinating safety reserve and engineering cost. The recommended thickness of 241 mm in this study is an engineering compromise obtained

based on this multi-objective trade-off logic. The representative finite element cases and the optimization solution set have different analytical functions. The representative cases are mainly used to reveal the variation in structural response with strengthening parameters under typical thickness schemes, whereas the optimization solution set is used to characterize the distribution of non-dominated schemes under multi-objective constraints. Their combination ensures both the traceability of data sources and the interpretability of the recommended thickness.

UHPC infill strengthening has good application potential for small-span concrete arch bridges, but its engineering implementation still requires attention to interface treatment, construction quality control, and long-term performance verification. First, the interface between UHPC and the existing concrete should be treated by roughening, cleaning, wetting, or planting reinforcement to ensure reliable composite action between the strengthening layer and the original structure [17]. Second, the cavity shape between arch ribs is often irregular; therefore, the actual geometric boundary should be verified through field remeasurement before construction to avoid inconsistency between the designed thickness and the castable space. Third, because UHPC has a low water-to-binder ratio and a high cementitious material content, shrinkage restraint and temperature effects should not be ignored. Studies on composite members also indicate that interface bonding and curing conditions can affect the cooperative mechanical behavior after strengthening [22,23]. Therefore, early-age cracking risk should be controlled through proper curing, staged construction, and necessary detailing measures.

A methodological limitation concerns the quantitative validation of the response mapping. The comparisons of the representative cases do not provide an independent estimate of mapping error. Such an assessment would require comparisons with finite-element results that were not used to construct the mapping.

This study remains a parameter optimization study based on finite element analysis and intelligent optimization, and the applicability of its conclusions is affected by model assumptions, material parameters, and loading conditions. The present work mainly considers deflection and stress responses under short-term static actions, while UHPC shrinkage and creep, temperature gradients, interface bond degradation, and long-term fatigue effects have not been fully incorporated. The optimization objectives mainly focus on mechanical performance and material consumption, without including construction duration, carbon emissions, traffic disturbance, maintenance cost, and life-cycle cost. Future studies may further densify the thickness samples within the range of 235–245 mm and incorporate life-cycle cost, carbon emissions, and construction disturbance into the objective functions, thereby forming a more comprehensive safety–economy–environment collaborative optimization model.

## 6. Conclusions

This study focused on the overall UHPC infill strengthening of an existing small-span concrete arch bridge. On the basis of clarifying the applicability of the strengthening scheme, a performance–material-consumption multi-objective optimization model was established with mid-span deflection, arch-springing compressive stress, and UHPC consumption as the objectives. The NSGA-III algorithm was then used to optimize the infill thickness. Based on representative finite element cases and non-dominated solution set analysis, the following conclusions can be drawn.

(1) A performance–material-consumption three-objective optimization model for the investigated concrete arch bridge was established by selecting the maximum control thickness of UHPC infill as the primary design variable and minimizing mid-span deflection, arch-springing compressive stress, and UHPC consumption. The model

incorporates structural performance improvement and material consumption into the same decision space, providing a quantitative multi-objective basis for parameter design using high-performance strengthening materials.

(2) For the investigated bridge and under the considered loading conditions, the representative finite element results indicate that UHPC infill strengthening can effectively improve the deformation and critical-section stress responses. The mid-span deflection and arch-springing compressive stress of the unstrengthened structure are 12.59 mm and 10.33 MPa, respectively. After strengthening, the mid-span deflection of the representative schemes decreases to 7.38–7.77 mm, and the arch-springing compressive stress decreases to 6.64–7.36 MPa, demonstrating improved stiffness and stress responses for the investigated case.

(3) As UHPC consumption increases, the structural deflection and arch-springing compressive stress generally decrease, but the mechanical benefit gained from further material addition gradually diminishes, showing an evident diminishing marginal benefit. From Scheme 4 to Scheme 6, UHPC consumption increases by approximately 12.51%, whereas the deflection is further reduced by only about 1.86% and the arch-springing compressive stress by only about 2.64%. This indicates that excessive thickening or expansion of the infill region is inefficient in terms of material utilization.

(4) Within the six reported cases, this thickness represents a compromise between the calculated structural responses and UHPC consumption. This scheme corresponds to a mid-span deflection of 7.52 mm, an arch-springing compressive stress of 6.82 MPa, and a UHPC consumption of 19.83 $m^3$. Compared with the unstrengthened state, the deflection and stress are reduced by approximately 40.27% and 33.98%, respectively, achieving a favorable balance between performance improvement and material consumption.

(5) The recommended thickness is specific to the investigated bridge and should be understood as the maximum control thickness within the arch-shaped cavity between its arch ribs, rather than as a generally applicable design value. Further experimental studies and additional bridge cases with different geometries, material properties, boundary conditions, and loading characteristics are required to validate the broader applicability of the proposed method.

**Author Contributions:** Conceptualization, X.L. and Y.D.; methodology, X.L. and Y.D.; software, X.L. and Y.Z.; validation, Y.Z. and J.Z.; formal analysis, X.L.; investigation, X.L.; resources, X.L. and Y.D.; data curation, J.Z.; writing—original draft preparation, X.L. and Y.D.; writing—review and editing, X.L. and J.Z.; visualization, J.Z.; supervision, Y.D.; project administration, Y.D.; funding acquisition, Y.Z. and Y.D. All authors have read and agreed to the published version of the manuscript.

**Funding:** This research was funded by the Innovation Project of Huadong Engineering Corporation Limited, PowerChina, grant number KY2024-JZ-02-22. This work was also funded by the National Natural Science Foundation of China, grant number 52378288.

**Data Availability Statement:** The data that support the findings of this study are available from the corresponding author upon reasonable request.

**Acknowledgments:** We sincerely thank the anonymous reviewers for their thorough evaluation and helpful feedback on this work.

**Conflicts of Interest:** The authors declare that this study received funding from the Innovation Project of Huadong Engineering Corporation Limited, PowerChina and the National Natural Science Foundation of China. The funder was not involved in the study design, collection, analysis, interpretation of data, the writing of this article or the decision to submit it for publication. Authors X.L., J.Z. and Y.Z. were employed by the company Huadong Engineering Corporation Limited, PowerChina. The

remaining authors declare that the research was conducted in the absence of any commercial or financial relationships that could be construed as a potential conflict of interest.

## References


1. Sarhosis, V.; De Santis, S.; de Felice, G. A review of experimental investigations and assessment methods for masonry arch bridges. *Struct. Infrastruct. Eng.* **2016**, *12*, 1439–1464. [CrossRef]
2. Fan, C.; Zheng, Y.; Wang, B.; Zhou, Y.; Sun, M. Damage identification method for tied arch bridge suspender based on quasi-static displacement influence line. *Mech. Syst. Signal Process.* **2023**, *200*, 110518. [CrossRef]
3. Bouzas, O.; Conde, B.; Matos, J.; Solla, M.; Cabaleiro, M. Reliability-based structural assessment of historical masonry arch bridges: The case study of Cernadela bridge. *Case Stud. Constr. Mater.* **2023**, *18*, e02003. [CrossRef]
4. Zizi, M.; Chisari, C.; De Matteis, G. Effects of pre-existing damage on vertical load-bearing capacity of masonry arch bridges. *Eng. Struct.* **2024**, *300*, 117205. [CrossRef]
5. Drosopoulos, G.; Stavroulakis, G.; Massalas, C.V. FRP reinforcement of stone arch bridges: Unilateral contact models and limit analysis. *Compos. Part B Eng.* **2007**, *38*, 144–151. [CrossRef]
6. Sumon, S.K. Innovative retrofitted reinforcement techniques for masonry arch bridges. *Proc. Inst. Civ. Eng.-Bridge Eng.* **2005**, *158*, 91–99. [CrossRef]
7. Zhang, K.; Li, D.; Shen, X.; Hou, W.; Li, Y.; Xue, X. Research on strengthening stone arch bridge with CFRP rebars. *Int. J. Build. Pathol. Adapt.* **2023**, *41*, 1014–1028. [CrossRef]
8. Scattarreggia, N.; Salomone, R.; Moratti, M.; Malomo, D.; Pinho, R.; Calvi, G.M. Collapse analysis of the multi-span reinforced concrete arch bridge of Caprigliola, Italy. *Eng. Struct.* **2022**, *251*, 113375. [CrossRef]
9. Yuan, S.; Chen, W.; Yang, F.; He, T.; Liu, G. Reinforcement analysis of rigid hangers for existing old arch bridges: A case study of Ling Bridge. *Int. J. Steel Struct.* **2019**, *19*, 1743–1754. [CrossRef]
10. Huang, H.D.; Xiang, Z.F.; Liu, J.F.; Lin, X.F. Study on internal force distribution method of co-section for arch bridges strengthening. *J. Chongqing Jiaotong Univ. (Nat. Sci.)* **2008**, *27*, 200–203. (In Chinese)
11. Liao, B.H.; Wang, G.D. Research and application of a new strengthening method for arch bridges. *Highway* **2006**, *10*, 34–37. (In Chinese)
12. Lv, Y.H.; Shi, J.Z.; Jiang, Z. Study on strengthening method of two-way curved arch bridges. *Technol. Highw. Transp.* **2005**, *4*, 117–118. (In Chinese)
13. Xu, J.Y.; Yuan, H.Q.; Wang, J. New strengthening measures for double-curved arch bridges. *J. Wuhan Urban Constr. Inst.* **2001**, *18*, 14–17. (In Chinese)
14. Chen, F.; Gong, H.H. Strengthening practice of double-curved arch bridges. *Highw. Automot. Appl.* **2011**, *1*, 135–138. (In Chinese)
15. Ademović, N. Structural assessment & strengthening of the first singe-arch RC bridge in Sarajevo, BIH. *Eng. Struct.* **2021**, *235*, 112002. [CrossRef]
16. Hamed, E.; Chang, Z.-T.; Rabinovitch, O. Strengthening of reinforced concrete arches with externally bonded composite materials: Testing and analysis. *J. Compos. Constr.* **2015**, *19*, 04014031. [CrossRef]
17. Gandelli, E.; Faccin, E.; Faini, S.; Facconi, L.; Lomiento, G.; Minelli, F. Seismic retrofit of a reinforced concrete arch bridge using low-mass tuned mass dampers. *J. Bridge Eng.* **2026**, *31*, 05026004. [CrossRef]
18. Wang, Z.; Yang, J.; Zhou, J.; Yan, K.; Zhang, Z.; Zou, Y. Strengthening of existing stone arch bridges using UHPC: Theoretical analysis and case study. *Structures* **2022**, *43*, 805–821. [CrossRef]
19. Yang, J.; Chen, R.; Zhang, Z.; Zou, Y.; Zhou, J.; Xia, J. Experimental study on the ultimate bearing capacity of damaged RC arches strengthened with ultra-high performance concrete. *Eng. Struct.* **2023**, *279*, 115611. [CrossRef]
20. Song, J.; Li, B.; Kong, L.; Qin, D.; Zhu, C.; Kuang, Y.; Shan, A. Effect of interface treatment on the flexural performance of existing RC bridge beams strengthened with UHPC. *Front. Mater.* **2024**, *11*, 1361647. [CrossRef]
21. Du, J.; Meng, W.; Khayat, K.H.; Bao, Y.; Guo, P.; Lyu, Z.; Abu-Obeidah, A.; Nassif, H.; Wang, H. New development of ultra-high-performance concrete (UHPC). *Compos. Part B Eng.* **2021**, *224*, 109220. [CrossRef]
22. Fehling, E.; Schmidt, M.; Walraven, J.; Leutbecher, T.; Fröhlich, S. *Ultra-High Performance Concrete UHPC: Fundamentals, Design, Examples*; Ernst & Sohn: Berlin, Germany, 2014.
23. ACI Committee 239. *ACI PRC-239-18: Ultra-High-Performance Concrete: An Emerging Technology Report*; American Concrete Institute: Farmington Hills, MI, USA, 2018.
24. Graybeal, B.A. *Material Property Characterization of Ultra-High Performance Concrete*; FHWA-HRT-06-103; Federal Highway Administration: McLean, VA, USA, 2006.
25. Habel, K.; Denarié, E.; Brühwiler, E. Experimental investigation of composite ultra-high-performance fiber-reinforced concrete and conventional concrete members. *ACI Struct. J.* **2006**, *103*, 93–101. [CrossRef]

26. Hussein, L.; Amleh, L. Structural behavior of ultra-high performance fiber reinforced concrete-normal strength concrete or high strength concrete composite members. *Constr. Build. Mater.* **2015**, *93*, 1105–1116. [CrossRef]
27. García-Segura, T.; Penadés-Plà, V.; Yepes, V. Sustainable bridge design by metamodel-assisted multi-objective optimization and decision-making under uncertainty. *J. Clean. Prod.* **2018**, *202*, 904–915. [CrossRef]
28. Deb, K.; Jain, H. An evolutionary many-objective optimization algorithm using reference-point-based nondominated sorting approach, part I: Solving problems with box constraints. *IEEE Trans. Evol. Comput.* **2014**, *18*, 577–601. [CrossRef]
29. Deb, K.; Pratap, A.; Agarwal, S.; Meyarivan, T. A fast and elitist multiobjective genetic algorithm: NSGA-II. *IEEE Trans. Evol. Comput.* **2002**, *6*, 182–197. [CrossRef]
30. Das, I.; Dennis, J.E. Normal-boundary intersection: A new method for generating the Pareto surface in nonlinear multicriteria optimization problems. *SIAM J. Optim.* **1998**, *8*, 631–657. [CrossRef]
31. Zitzler, E.; Deb, K.; Thiele, L. Comparison of multiobjective evolutionary algorithms: Empirical results. *Evol. Comput.* **2000**, *8*, 173–195. [CrossRef]
32. Coello Coello, C.A.; Lamont, G.B.; Van Veldhuizen, D.A. *Evolutionary Algorithms for Solving Multi-Objective Problems*, 2nd ed.; Springer: New York, NY, USA, 2007.
33. Patidar, V.; Labi, S.; Sinha, K.C.; Thompson, P.D. *Multi-Objective Optimization for Bridge Management Systems*; NCHRP Report 590; Transportation Research Board: Washington, DC, USA, 2007.
34. Frangopol, D.M.; Soliman, M. Life-cycle of structural systems: Recent achievements and future directions. *Struct. Infrastruct. Eng.* **2016**, *12*, 1–20. [CrossRef]
35. *JTG/T J21-01-2015*; Specification for Load Testing of Highway Bridges. China Communications Press: Beijing, China, 2015. (In Chinese)
36. *JTG D60-2015*; General Specifications for Design of Highway Bridges and Culverts. China Communications Press: Beijing, China, 2015. (In Chinese)


**Disclaimer/Publisher's Note:** The statements, opinions and data contained in all publications are solely those of the individual author(s) and contributor(s) and not of MDPI and/or the editor(s). MDPI and/or the editor(s) disclaim responsibility for any injury to people or property resulting from any ideas, methods, instructions or products referred to in the content.